# Discretely tunable laser based on filtered feedback for telecommunication applications

# Discretely Tunable Laser Based on Filtered Feedback for Telecommunication Applications

Boudewijn Docter, *Member, IEEE*, Jose Pozo, *Member, IEEE*, Stefano Beri, Ilya V. Ermakov, *Student Member, IEEE*, Jan Danckaert, *Member, IEEE*, Meint K. Smit, *Fellow, IEEE*, and Fouad Karouta, *Senior Member, IEEE*

***Abstract*—A novel discretely tunable laser based on filtered feedback is presented. The semiconductor device consists of a Fabry–Perot laser with deeply etched broadband distributed Bragg reflector mirrors. Single-mode operation is achieved by using feedback from an integrated filter. This filter contains an arrayed waveguide grating wavelength router and a semiconductor optical amplifier gate array. Design, simulation, and the first characterization results of this new integrated filtered-feedback tunable laser device are presented. It shows a combination of a simple and robust switching algorithm with good wavelength stability. A rate equation model predicts that a properly designed device can switch within 1 ns. The fast switching and reduced control complexity makes the device very promising for various advanced applications in optical telecommunication networks.**

***Index Terms*—Filtered feedback, packet switching, photonic integrated circuits, semiconductor lasers, tunable lasers.**

## I. Introduction

TUNABLE lasers are widely used in telecommunication networks nowadays for flexible reconfiguration of the network and in wavelength-division multiplexing (WDM) systems, where a single tunable laser can be used as a replacement for all fixed wavelengths lasers in the network. [1], [2].

Most continuously tunable lasers require complex control electronics to stabilize the laser output signal. A laser based on tunable distributed Bragg reflector (DBR) mirrors, for example, needs accurate current control in at least four sections: the main laser gain section, the front and rear mirrors, and a phase section to prevent unwanted mode-hops. To address a prescribed wavelength, all tuning currents have to be set precisely according to a tuning table. Switching to another wavelength requires a change in the current settings. This will incur slow thermal transients and complex control algorithms are required to keep the wavelength fixed during these transients [3].

The new integrated filtered-feedback tunable laser (IFF-TL) demonstrated in this paper circumvents these drawbacks. Since the device consists of a Fabry–Perot (FP) laser without any tuning elements in the main laser cavity, the device is very stable against temperature fluctuations due to tuning currents. The tuning currents have a very wide tolerance and the control mechanism is therefore much simpler. This potentially reduces the cost of this device compared to conventional tunable lasers.

Manuscript received September 14, 2009; revised November 23, 2009; accepted November 29, 2009. Date of publication January 8, 2010; date of current version October 6, 2010. This work was supported by the Dutch Technology Foundation STW, by the Research Foundation Flanders (FWO), and by the Interuniversity Attraction Poles program of the Belgian Science Policy Office under Grant IAP P6-10.

B. Docter, J. Pozo, and M. K. Smit are with the COBRA Research Institute, Eindhoven University of Technology, 5600 MB Eindhoven, The Netherlands (e-mail: b.docter@tue.nl).

S. Beri, I. V. Ermakov, and J. Danckaert are with the Department of Physics and the Department of Applied Physics and Photonics, Vrije Universiteit Brussel, 1050 Brussels, Belgium (e-mail: iermakov@vub.ac.be).

F. Karouta is with Australian National University, Canberra A.C.T. 0200, Australia.

Color versions of one or more of the figures in this paper are available online at http://ieeexplore.ieee.org.

Digital Object Identifier 10.1109/JSTQE.2009.2038072

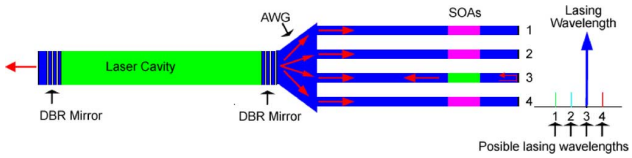


Fig. 1. Schematic of the IFF-TL device.

The principle of the IFF-TL was first described by Docter *et al*. [4] and then experimentally demonstrated by Matsuo *et al*. [5]. In this study, two coupled microring filters were used for controlling the wavelength. It was shown that with this approach, the frequency drift due to temperature changes can be reduced from 7 GHz to less than 1 GHz. In another publication by Fürst *et al*. [6], a ring resonator laser was forced to operate in a single-laser mode by using filtered feedback from a tunable narrow-band DBR grating. In their paper, the authors report a switching speed of 450 ps. However, in both these devices the filter component was controlled by one or two analog input signals, making the operation of the devices still sensitive to temperature fluctuations. In an earlier paper [7], we have shown that semiconductor optical amplifiers (SOAs) can effectively be used as gate switches in discretely tunable lasers. These short gate switches allow for switching times of a few ns in a long extended cavity laser. Incorporating them in a filtered-feedback scheme can significantly reduce the switching speed.

In this paper, we present a laser, which uses a compact arrayed waveguide grating (AWG) integrated with short SOA gate switches for controlling the wavelength. We demonstrate that the filtered-feedback principle in combination with an AWG and an SOA gate switch array allows for simple and stable tuning. To our knowledge the device presented in this paper is the first device that operates in a quasidigital manner, making it a very promising device for large-scale application in fiber networks.

## II. Operating Principle

A schematic picture of the novel IFF-TL is shown in Fig. 1. An FP laser is formed by an SOA and two deeply etched DBR mirrors. The laser cavity length is chosen such that the mode spacing equals the channel spacing in the standard International Telecommunication Union (ITU) grid used for telecom applications [8], e.g., 50 or 100 GHz.

The FP laser is coupled to an AWG filter [9] that splits the light of the FP laser in several waveguide branches. Each branch

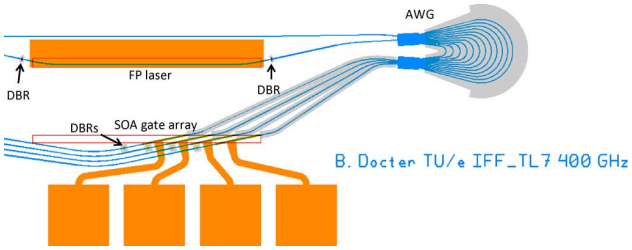


Fig. 2. Layout of IFF-TL device. The positions of the different components are indicated in the figure.

contains an SOA that works as an optical gate. When the SOA is not biased, it will absorb the light, but when put in forward bias, the light will be transmitted or even amplified. The light is then reflected either by a cleaved chip facet, another DBR mirror or any other form of broadband mirror, and fed back through the AWG into the FP laser. The feedback light causes the laser mode with the largest feedback strength to dominate over the other modes and single-mode operation is achieved. The feedback strength is controlled by the gates in the feedback branches. The output light leaves the chip through the opposite DBR mirror.

The concept of filtered-feedback has many advantages over other tunable laser concepts. Compared to tunable DBR lasers [10]–[12], the main difference is that the tuning mechanism is outside the main laser cavity. This means that there is no change in refractive index in the main FP laser cavity while switching the wavelength. Therefore, the wavelength stability is improved and control schemes are simpler. The limitation is that the device can only operate at a fixed set of wavelengths.

The effect of temperature-induced wavelength drift due to changing tuning currents is very small. A good comparison of these temperature effects in a conventional (ring-resonator based) tunable laser and a filtered-feedback tunable laser is given in [5].

Compared to conventional AWG lasers [7], [13], the main advantage of the IFF-TL device is that the AWG is not part of the main laser cavity. Losses caused by the AWG do not have to be compensated by the gain section to reach lasing threshold. Any nonuniformity in the transmission of the AWG channels only translates into a lower feedback signal, which potentially can slow down the switching speeds for these channels, but the threshold current is not changed. Therefore, the carrier density in the laser cavity will be the same, which results in a very stable wavelength.

Theoretically, the device can switch between any two wavelengths without addressing unwanted wavelengths. This prevents the so-called "dark-tuning," which requires blanking of the laser output while switching the wavelength. However, this was not experimentally confirmed yet.

## III. Device Design

### A. FP Laser

The layout that was used for the IFF-TL devices is shown in Fig. 2. The main element of the IFF-TL is an 822-$\mu$m-long FP laser with 2-period deeply etched DBR mirrors. A detail of the FP laser is shown in Fig. 3. For this device, we use an

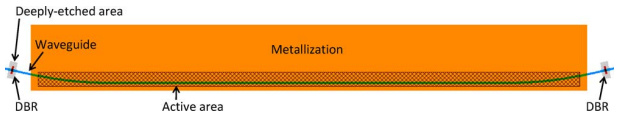


Fig. 3. Detail of the chip layout showing the FP laser.

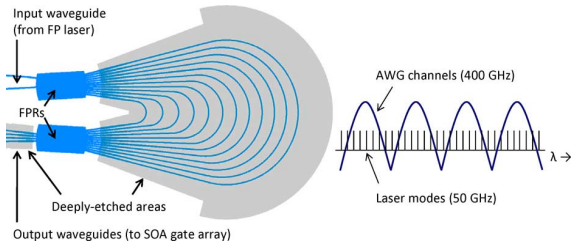


Fig. 4. Detail of the chip layout showing the AWG filter. The deep- and shallow-etched areas are indicated in the figure (FPR = free propagation region). The possible FP-laser modes and AWG filter response are given in the graph on the right.

active–passive integration scheme based on a three-step growth technique as described in [14] and [15]. The waveguides cross the active–passive interface under an angle to reduce any possible reflections from the butt joint. The 2-period DBR mirrors are deeply etched, while the rest of the structure consists of shallow etched waveguides.

The DBR mirrors allow us to control the laser cavity length very accurately. This is important since the mode spacing $\Delta\lambda$ is given by the following formula:

$$\Delta\lambda = \frac{\lambda^2}{2N_g L_{\mathrm{cav}}} \tag{1}$$

where $N_g$ is the group index of the waveguide ($N_g \approx 3.65$) and $\lambda$ is the central wavelength (1.55 $\mu$m). The cavity length $L_{\mathrm{cav}}$ of 822 $\mu$m therefore corresponds to a mode spacing of 0.4 nm or 50 GHz. The exact position of the FP laser modes can be tuned by changing the operating temperature of the laser.

### B. AWG Filter

The AWG filter was designed using a deep-shallow double etching technique as described in [16]. The layout of the AWG device is shown in Fig. 4. In this design, the four-channel AWG connected to the FP laser has a channel spacing of 3.2 nm or 400 GHz. This relatively coarse channel spacing keeps the AWG compact. The AWG can be designed so that there is an integer number of FP modes in each AWG channel. This is schematically shown in right part of Fig. 4.

### C. SOA Gate Array

In the feedback branches, an array of 100-$\mu$m-long SOA gates has been implemented. A detail of the chip layout showing the SOA gate array is given in Fig. 5. Directly after the gates, there are 3-period DBR mirrors that reflect about 85% of the light back through the gates and the AWG to provide the filtered-feedback signal. These DBR mirrors also let a small portion of the light pass that can be used for characterization purposes.

The relatively short SOAs provide only 1 or 2 dB gain when they are biased around 10 mA. However, when the gates are not

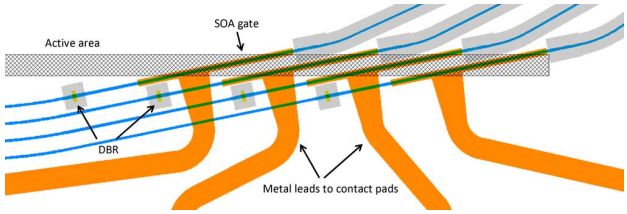


Fig. 5. Detail of the chip layout showing the SOA gate array.

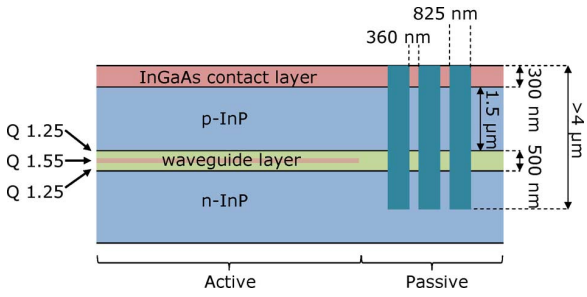


Fig. 6. Schematic side view of deeply etched DBR mirror filled with BCB. The active layer consists of a 120-nm-thick bulk layer of InGaAsP with a bandgap corresponding to $\lambda = 1.55$ $\mu$m (Q1.55). This layer is embedded in a Q 1.25 passive waveguide layer (see Section V).

biased, virtually all the light is absorbed, effectively creating a large difference in feedback strength between the different wavelengths. The current through the gates can also be used to influence the phase of the feedback signal. This can be used to select the right mode when multiple FP modes are passed through each AWG channel.

### *D. Deeply Etched DBR Mirrors*

The deeply etched DBR mirrors that are used to form the FP laser are schematically shown in Fig. 6. These DBR mirrors provide high reflectivity over the full-gain spectrum [17]. After etching the waveguides and mirrors, the device is planarized with a bisbenzocyclobutene-based polymer (BCB) (refractive index $n_{\mathrm{BCB}} = 1.54$). The BCB also penetrates in the gaps of the DBR mirrors. We use a third-order DBR design, where the length of each section equals (3/4)$\lambda/N$ ($N$ is the effective index of the mode in each material). This means that the gaps that are etched in the waveguides are 825 nm wide and the semiconductor left in between the gaps is 360 nm wide. Compared to a first-order design, the third-order design makes it easier to obtain the necessary etch depth.

In the IFF-TL device described in this paper, we used 2-period DBR mirrors to form the FP laser cavity and 3-period DBR mirrors in the feedback branches to reflect the light back to the FP laser. The calculated reflection and transmission spectra of such mirrors are shown in Fig. 7. The 2-period mirror provides about 70% reflectivity, but still allows approximately 20% of the light to pass through the mirror.

## IV. Filtered-Feedback Model

In order to demonstrate the operating principle, as well as testing the potential performance of the IFF-TL device, we performed numerical simulations based on an extended Lang–

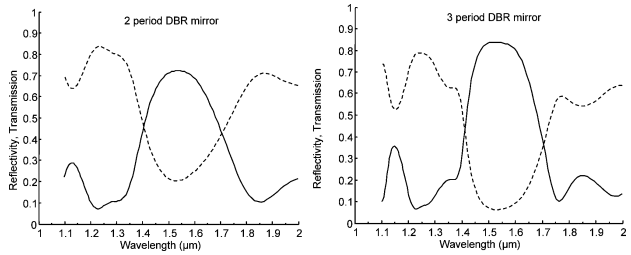


Fig. 7. 3-D finite-difference time-domain (FDTD) simulation of the reflection (solid lines) and transmission (dashed lines) of a 2-period deeply etched DBR mirror (left) and a 3-period deeply etched DBR mirror (right).

Kobayashi model [18], [19]. This model consists of a set of delay differential equations (DDEs) for the complex slowly varying field amplitudes $E_m$ of each laser mode and the average carrier inversion $N$ [normalized at transparency $N_0$] in the FP cavity

$$\dot{E}_m = \frac{1}{2}(1+i\alpha)\left[\frac{g_m(N(t)-N_0)}{1+S|E_m|^2+C\sum_{k\neq m}|E_k|^2}-\frac{1}{\tau_m^{ph}}\right] \times E_m + \gamma_m F_m \tag{2}$$

$$\dot{F}_m = \Lambda E_m(t-\tau)e^{i\phi_m} + (i\Delta\omega_m - \Lambda)F_m \tag{3}$$

$$\dot{N} = \frac{I}{q} - \frac{N}{\tau_n} - g(N-N_0) \times \sum_{m=1}^{n}\left(\frac{|E_m|^2}{1+S|E_m|^2+C\sum_{k\neq m}|E_k|^2}\right) \tag{4}$$

where $\tau_m^{ph}$ and $g_m$ are, respectively, the photon lifetime and the differential gain for mode $m$. For simplicity, we assume equal gain $g = 1.5\times10^{-5}$ ns$^{-1}$ for all modes. Different modes in the cavity are coupled nonlinearly by saturation processes such as spectral hole burning that are modeled here by the phenomenological coefficients $S = C = 5\times10^{-7}$ and $\alpha = 5$ is the linewidth enhancement factor of the semiconductor material. The injection current is $I = 45$ mA, $q = 1.602\times10^{-19}$ is the electron charge and $\tau_n = 2$ ns is the carrier lifetime. Spontaneous emission of photons in the laser cavity has been included in the simulation by adding two white-Gaussian noise terms in the field equations.

The feedback is described in (3) in terms of feedback amplitudes $\gamma_m$, phases $\phi_m$ and delay time $\tau = 2L_{\mathrm{ext}}N_g/c = 46.2$ ps, where $L_{\mathrm{ext}} \approx 1.9$ mm is the length of external branches and $c$ is the speed of light in vacuum. In (3), the change of the group index in the SOA gate sections due to carrier injection is accounted for by the phase $\phi_m$.

The AWG in the feedback cavity is modeled as a Lorentzian filter with half width at half maximum $\Lambda = 200$ GHz and detuning $\Delta\omega_m = 0$, as described by (3), for the auxiliary dynamical variables $F_m$. Different values of the bias current on the SOA gates can be modeled with a choice of the feedback strength $\gamma$

$$\gamma = \frac{(1-R_{\mathrm{DBR}})}{\tau_{\mathrm{in}}}\sqrt{\frac{R_{\mathrm{DBR}}^{\mathrm{ext}}}{R_{\mathrm{DBR}}}}\cdot(1-A_{\mathrm{DBR}})^2\,T_{\mathrm{AWG}}^2\,A_{\mathrm{SOA}}^2 \tag{5}$$

where by $R_{\mathrm{DBR}}$ we consider the reflectivity of the DBR mirrors of the main cavity. There are also some scattering losses in the DBR mirrors ($R_{\mathrm{DBR}} + T_{\mathrm{DBR}} < 1$). These losses are

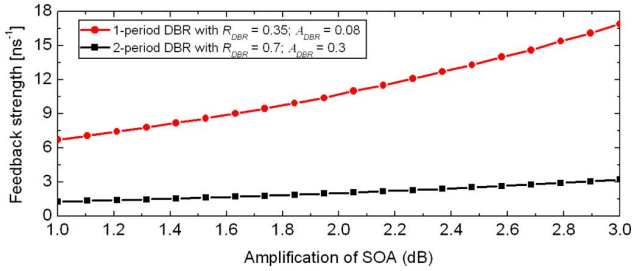


Fig. 8. Dependence of feedback strength $\gamma$ on SOA amplification. Parameters are $\tau_{\rm in} = 20$ ps, $R_{\rm DBR}^{\rm ext} = 0.85$, $T_{\rm AWG} = 0.316$.

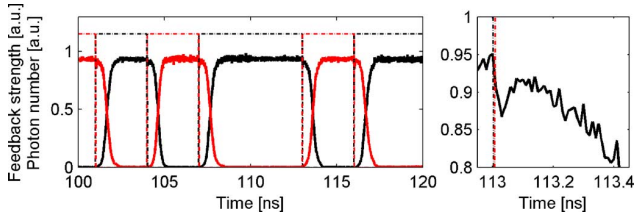


Fig. 9. Numerical simulations of switching sequence induced by modulation of the feedback parameters. Solid lines: power in mode 1 and mode 2, dashed lines: feedback strength in channel 1 and channel 2. The image on the right shows a detail of the switching dynamics, where the drop in output power is visible when the feedback is switched. Parameters are $\gamma_1 = \gamma_2 =$ 0–6 ns$^{-1}$, $\phi_1 = \phi_2 = 0$, $\tau_1^{\rm ph} = 1.999$ ps, $\tau_2^{\rm ph} = 2$ ps. The small difference in photon lifetime simulates slightly different propagation losses for the two modes.

accounted for in an absorption term $A_{\rm DBR}$. For the 2-period DBR mirror, which simulated reflection and transmission spectra, are given in Fig. 7, $A_{\rm DBR}$ is given by $1 - T_{\rm DBR}/(1 - R_{\rm DBR}) =$ 1–0.2/0.3 = 0.33. $\tau_{\rm in} = 2L_{\rm cav}N_g/c = 20$ ps is the roundtrip time of the main cavity, $R_{\rm DBR}^{\rm ext}$ is the reflectivity of the 3-period DBR mirror at the end of the feedback branches. $T_{\rm AWG}$ is the transmission of the AWG and $A_{\rm SOA}$ is the amplification of an SOA. In Fig. 8, we show the dependence of feedback strength $\gamma$ on amplification of the SOA for two different types of DBR mirrors. A lower DBR reflectivity leads to a larger feedback signal, which enhances the switching speed, as will be shown in the next paragraphs.

For the sake of simplicity, we illustrate the result in the simple, but not trivial case of two competing lasing modes of the FP cavity amplified by the feedback from two different AWG channels. Since we assume a flat gain spectrum, the lasing mode is selected by applying the feedback.

We induce mode switching by alternating the feedback parameters $\gamma_1$ and $\gamma_2$ between 0.0 and 6.0 ns$^{-1}$ in a pseudorandom way. Practically, this corresponds to forward biasing one of the SOA gates without biasing the other gates.

Time series of the mode-resolved power from simulations of (2)–(4) are shown in Fig. 9. The device lases in one mode when the corresponding gate is forward biased. When the feedback is moved to another channel, the operation switches to the other mode, because the effective gain of the corresponding mode is increased. The modal power rises and quenches the gain of the other mode. An evidence for this mechanism is shown in the inset of Fig. 9; when the feedback is removed from the lasing mode, its power suddenly drops as a consequence of a change in its effective gain. This mode keeps lasing (although with a lower efficiency) until the other mode—which is now favored by the presence of the feedback—takes over.

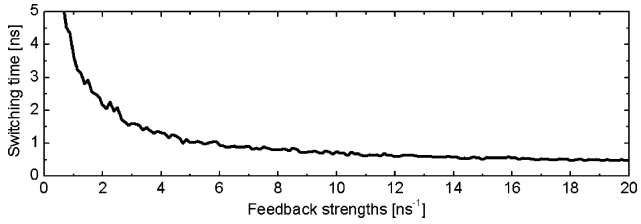


Fig. 10. Dependence of the switching time on the feedback strengths $\gamma_{1,2}$. Parameters are $\phi_1 = \phi_2 = 0$, $\tau_1^{\rm ph} = 1.999$ ps, $\tau_2^{\rm ph} = 2$ ps.

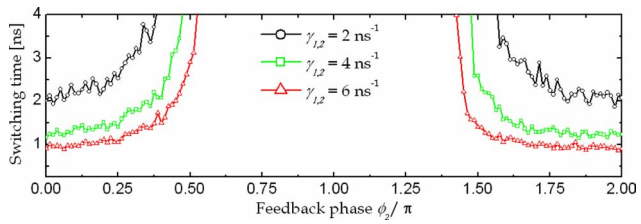


Fig. 11. Dependence of the switching time on the feedback phase $\phi_2$. Parameters are $\phi_1 = 0$, $\tau_1^{\rm ph} = 1.999$ ps, $\tau_2^{\rm ph} = 2$ ps.

The dependence of the switching time on the feedback strength is shown in Fig. 10. Here, we assumed that a switch is completed once the mode power reaches 90% of the total power. An average of ten switches is used.

As expected, an increase in the feedback intensity leads to a decrease of the switching time, as it increases the difference between the effective gain of the modes. The order of magnitude of the switching speed is in accordance with the measured switching speed of the ring-resonator based filtered-feedback devices presented in [5] and [6] and the AWG laser using the gate switches described in [7].

The dependence of the switching time on the phase of the feedback is shown in Fig. 11. It is clear that the switching time dramatically increases for feedback phases between $0.5\pi$ and $1.5\pi$, and that no switches are observed for feedback phases around $\pi$, because when the feedback field is out-of-phase with the lasing mode, the effective gain decreases, leading to a further suppression of the side mode instead of a switch.

In the current design, the bias current on the SOA gates can be used to influence the phase of the feedback light, since an increase in carrier density will lead to a change in refractive index. It is therefore possible to adjust the current so that the feedback phase is between 0 and $0.5\pi$ or $1.5\pi$ and $2.0\pi$. Note that the exact current setting is therefore very tolerant.

## V. Fabrication

The IFF-TL device was fabricated using an active–passive integration scheme developed in cooperation with JDS Uniphase [14], [15]. All layers are grown by metal–organic vapor-phase epitaxy (MOVPE). First, the active layer stack is grown on an n-doped substrate. The active layer is formed by a 120-nm-thick bulk InGaAsP layer (Q1.55, bandgap at $\lambda = 1.55$ $\mu$m) embedded in two 190-nm-thick InGaAsP (Q1.25, bandgap at $\lambda = 1.25$ $\mu$m) confinement layers. The active blocks are then covered by a

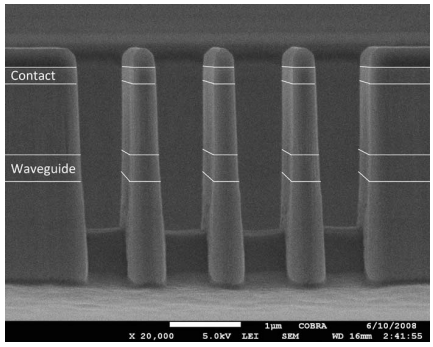


Fig. 12. Side-view SEM image of a deeply etched DBR mirror. The $SiO_2$ etching mask is still present. The white lines indicate the position of the contact layer and the waveguide layer (see also Fig. 6).

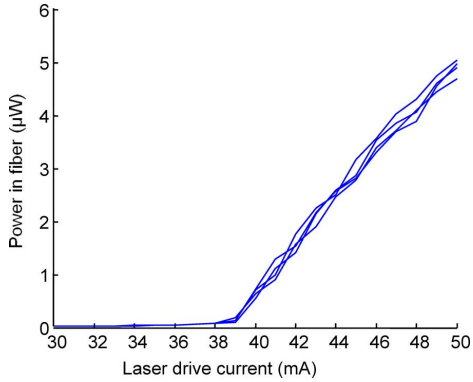


Fig. 13. *LI* curves of the IFF-TL device while forward biasing different gates at 10 mA. Note that *x*-axis scale starts at 30 mA.

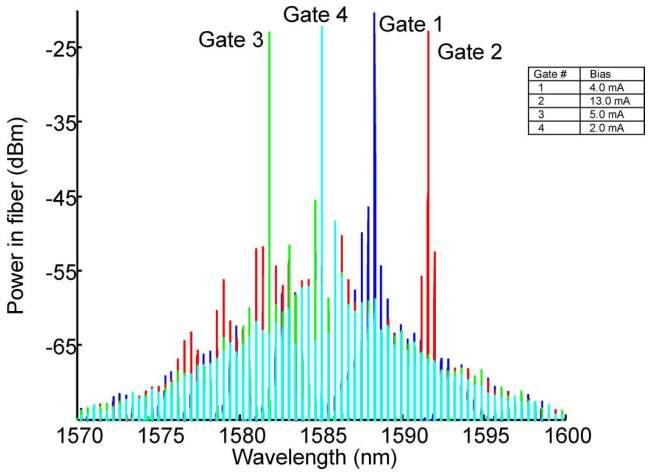


Fig. 14. Superimposed lasing spectra of the IFF-TL device while forward biasing the different gates. The laser was forward biased at 45 mA. The currents on the different gates are shown in the table.

lithography-defined $SiO_2$ layer and removed wet-chemically. Then, the passive Q1.25 waveguide layer is selectively grown (500 nm thick) in the second growth step. After removal of the $SiO_2$ mask layer the third and final growth step adds the common cladding and contact layers.

After the growth of the materials, the masking layers for the waveguide definition are applied. First, we deposit a 430-nm-thick $SiO_2$ layer by Plasma-enhanced chemical vapor deposition (PECVD) and then a 50 nm Cr layer is evaporated. The Cr layer allows us to combine the e-beam lithography (EBL) pattern required for the DBR mirrors with the optical lithography pattern required for the waveguides. This combined lithography process is described in [20]. A 320-nm-thick ZEP e-beam resist is applied and the DBR patterns are written using a Raith 150 e-beam system using 30 kV acceleration voltage. The DBR pattern is transferred into the Cr layer by $Cl_2$:$O_2$ inductively coupled plasma (ICP) etching. Then, the waveguide pattern is aligned by optical lithography on the DBR structures. This pattern is also transferred to the Cr layer, which then serves as an etching mask to open the 430-nm-thick $SiO_2$ layer in a CHF3 RIE process.

The device was fabricated using a double-etching technique. This enables the realization of shallow-etched and deeply etched waveguides using the same lithography pattern for the optical channels, avoiding strict alignment requirements. The shallow waveguides are used for low-loss interconnects, the SOAs and some parts of the AWG. The deeply etched waveguides are suitable for tight bends and DBR reflectors. The deep etching was done using a $Cl_2$:Ar:$H_2$ ICP etching process. This process offers straight and smooth sidewalls, which are necessary for the deeply etched DBR mirrors. An SEM image of a fabricated DBR mirror is shown in Fig. 12. The shallow SOA waveguides were later etched by $CH_4$:$H_2$ ICP etching.

After the etching, a 100 nm $SiO_2$ passivation layer is applied by PECVD and the chip is planarized using a single layer of BCB 3022-46. The planarization properties of the BCB are such that when spun at the right speed, hardly any back-etching is required to open the top of all the waveguides. Ti/Pt/Au p-contacts are added using e-beam evaporation and lift off. Then, an extra 1-$\mu$m-thick Au layer is electroplated on the large contacts to ensure uniform current injection. Finally, the sample is cleaved and fixed on a copper mount.

## VI. Characterization

### A. LI Characteristics

Fig. 13 shows the *LI* curves for the IFF-TL device operating at 15 °C. The device has an output waveguide with an angle of 7° with respect to the chip facet. This reduces the reflections from the edge of the chip. The light was collected using a lensed fiber and then split into two branches, one to record the output power and one to record the spectrum. The power collected in the fiber is quite low because of high coupling losses between the chip and the lensed fiber.

The different curves in Fig. 13 were recorded while forward biasing each of the gates separately with 10 mA of current. This provides only about 1–2 dB gain, due to the limited length of the gates. There is also one curve where no gate was opened. From the graphs, it is visible that the threshold current is not affected by the feedback light. This is a first indication that the carrier density in the laser stays constant while switching the channels, which is beneficial for the wavelength stability.

### B. Lasing Spectra

Fig. 14 shows the superimposed lasing spectra of the devices when operated at 45 mA. The text near the different laser peaks

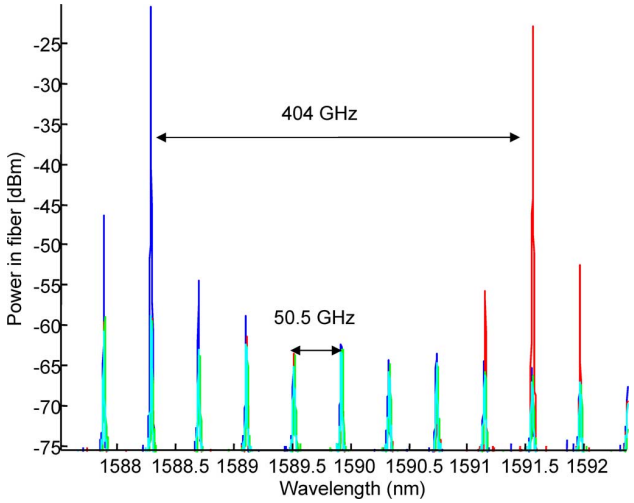


Fig. 15. Detail of the lasing spectra showing 50.5 GHz FP mode spacing and 404 GHz mode spacing between AWG channels 1 and 2.

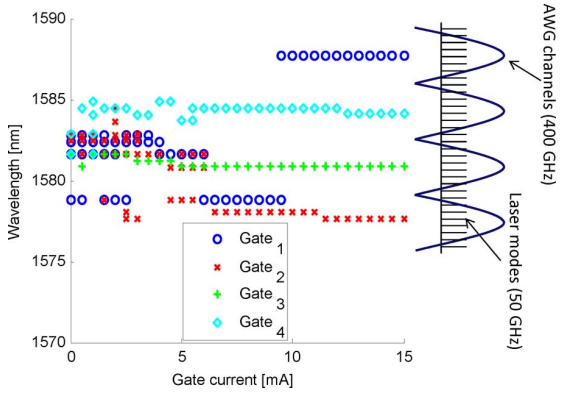


Fig. 16. Lasing wavelengths as a function of different gate bias currents. The inset on the right indicates the position of the AWG channels and the possible FP laser modes. The device was driven with 41 mA on the main laser contact.

indicates which gate was operated. The forward bias on the different gates was between 2 and 13 mA. We can clearly see single-mode operation for each of the channels. The SMSR for the various signals is at least 20 dB. This relatively low value is due to the fact that the passband of the AWG channels is much wider than the 50 GHz modespacing of the FP laser. The difference in transmission of this filter is therefore only small. Moving to a design with more densely spaced channels can improve the side-mode suppression ratio (SMSR).

In Fig. 15(a), smaller part of the spectrum is plotted. In this figure, we observe the subthreshold side modes that originate from the modes of the FP cavity. The mode spacing is 0.404 nm. This corresponds to a frequency spacing of 50.5 GHz, 1% deviation from the ITU spacing. The distance between the lasing channels is 404 GHz.

The plot in Fig. 15 clearly demonstrates the wavelength stability of the device. The FP side modes coincide exactly, no matter which gate is operated. This shows that the group index of the modes in the laser does not change, even though the gates are operated at different currents. This is a clear indication that the carrier density and the temperature in the main laser cavity are very stable, and therefore, we expect very little frequency drift after switching the laser.

It is commonly known that feedback in semiconductor lasers can cause complex dynamic behavior, and can finally lead to coherence-collapse. This is characterized by a large increase in relative intensity noise (RIN), accompanied by an increase in the laser linewidth. However, such regimes require a large feedback delay and/or strength (i.e., large $\tau$ and/or large amplification), which are unlikely in our design (short feedback cavity and short SOA gates). We did not directly address the RIN in our investigation, however, significant increases in the laser linewidth with the feedback were never observed.

In another experiment, the peak wavelengths were recorded using a wavelength meter (ANDO AQ6141). This device records the wavelength and power of the peaks in an arbitrary spectrum. In Fig. 16, the lasing wavelengths are plotted as a function of the forward bias on the different gates, while operating one of the gates at the time. Also, the possible FP-laser modes and the AWG channel passbands are plotted as a reference. The bias current on the main laser cavity was reduced to 41 mA because the lasing wavelength seems to be the least sensitive to fluctuations in the gate currents when operated close to threshold.

Initially, at low gate bias currents, the laser operates at random wavelengths, probably determined by reflections from wavelengths that fall in between two AWG channels. As the bias current is increased the laser becomes single mode. Within the 400 GHz AWG channels, 50 GHz mode-hops are visible. These mode-hops are caused by a change of feedback phase due to the changing gate currents. The wavelength that has the most favorable phase matching will lock the laser. However, the lasing wavelength is usually stable over a wide range in gate currents. This shows that the control of the laser is not very critical and can be realized with relatively simple electronics.

## VII. Discussion

A novel concept in the field of tunable lasers has been demonstrated. In this section, the most important properties of the IFF-TL will be summarized and put into perspective with respect to the many alternatives that are commercially available nowadays.

### A. Switching Speed

The theoretical investigation of the filtered-feedback concept shows that nanosecond wavelength switching speeds are possible. Previous experiments with devices operating with a similar feedback concept [5], [6] showed confirmation of the very fast switching speeds that can be obtained using feedback to switch an FP laser. Full dynamic characterization of the current device is still in progress.

The ns switching speed will make the device suitable for packet switching applications. Integrating the tunable laser with a wavelength converter and a passive wavelength router can result in a very fast optical network switch. Furthermore, the device could, in principle, also be integrated with optical header processors, opening the way toward all-optical packet switching.

### B. Temperature Effects

Because the SOA gates are placed outside the laser cavity, temperature changes due to the switching currents do not affect the lasing wavelength. This is shown in Fig. 15. The temperature changes of course also influence the phase of the feedback. However, the theoretical investigation in Section IV showed that there is a large operating regime in which small phase changes do not affect the switching speed, and the graphs in Fig. 16 show stable wavelengths over a large range in gate currents. We, therefore, believe that thermal transients due to switching currents will have very little effect on the lasing wavelength.

Wavelength drift due to changes in temperature can be a big problem in tunable lasers using integrated tunable DBR mirrors that are tuned by current injection [21]. A control scheme that precompensates these temperature drifts complicates the control electronics significantly. Matsuo *et al*. [5] already demonstrated a reduction in optical frequency drift from 7 to 1 GHz in a ring-resonator based IFF-TL device. We believe that the AWG-based IFF-TL can reduce these temperature drifts even further.

### C. Control Electronics

Keeping the control electronics simple is important since the cost of the electronics is a major part of the total price of the tunable lasers that are commercially available nowadays. A reduction of these costs would make this device more interesting in high volume, low-cost applications, like metro and access networks.

Existing tunable lasers can address more than 100 WDM channels with only four analog control currents (gain, two tunable DBR mirrors, and a phase control section). However, to find the right combination of current settings requires a complex tuning table and intelligent electronics.

The quasidigital operation scheme of the AWG-based IFF-TL reduces the complexity of the electronics required to control the laser. However, the total number of control currents can become large as the number of wavelength channels increases.

### D. Number of Wavelengths

The device presented in this paper has four wavelength channels determined by the AWG. The concept can easily be extended to a larger number of wavelengths, but increasing the density of the AWG channels also results in a larger AWG. The surface of the AWG roughly increases by a factor of 1.5 when the channel spacing is reduced by a factor of 2. With a 50 GHz AWG, the number of wavelengths in the device can be increased to 32.

### E. Output Power

The output power of the device in the experiments reported in this paper is relatively low because of the high reflectivity of the front DBR mirror and because the coupling efficiency from the chip to the lensed fiber that was used to collect the light is not very good. The output power of this device can be increased by integrating a booster SOA in the output waveguide. Also changing the laser design so that the output DBR mirror has a lower reflectivity will improve the laser power. The 800 $\mu$m cavity should, in principle, allow for at least 10 mW of output power.

### F. Conclusion and Outlook

A novel discretely tunable laser based on filtered feedback was presented. A DDE model was developed that allows us to predict switching speeds below 1 ns. We also found that the feedback phase has a large range for which fast switching can be obtained. The predicted dynamical behavior still has to be confirmed with high-speed measurements, but the static characterizations already show that the device has broad operating regimes.

The new concept of the IFF-TL combines high switching speeds with simple wavelength control. While the latter promises a reduction in cost of the control electronics compared to continuously tunable lasers, we believe that the fast switching speed is the biggest advantage of this new device. Together with the fact that the device can be integrated with other active and passive components, we expect that fast switching will enable new applications in packet routing techniques for all-optical telecommunication networks.

## References


[1] L. A. Coldren, "Monolithic tunable diode lasers," *IEEE J. Sel. Topics Quantum Electron.*, vol. 6, no. 6, pp. 988–999, Nov./Dec. 2000.

[2] J. Buus and E. J. Murphy, "Tunable lasers in optical networks," *J. Lightw. Technol.*, vol. 24, no. 1, pp. 5–11, Jan. 2006.

[3] L. A. Coldren, G. A. Fish, Y. Akulova, J. S. Barton, L. Johansson, and C. W. Coldren, "Tunable semiconductor lasers: A tutorial," *J. Lightw. Technol.*, vol. 22, no. 1, pp. 193–202, Jan. 2004.

[4] B. Docter, S. Beri, F. Karouta, and M. K. Smit, "Semiconductor laser device," Int. Patent #PCT/NL/2008/000185, filed Aug. 1, 2008.

[5] S. Matsuo, T. Segawa, T. Kakitsuka, T. Sato, R. Takahashi, H. Suzuki, B. Docter, F. Karouta, and M. K. Smit, "Integrated filtered feedback tunable laser using double-ring-resonator-coupled filter," in *Proc. IEEE 21st Int. Semicond. Laser Conf. (ISLC 2008)*, Sep.14–18,, pp. 155–156.

[6] S. Furst, S. Yu, and M. Sorel, "Fast and digitally wavelength-tunable semiconductor ring laser using a monolithically integrated distributed Bragg reflector," *IEEE Photon. Technol. Lett.*, vol. 20, no. 23, pp. 1926–1928, Dec. 2008.

[7] A. La Porta, M. J. R. Heck, X. J. M. Leijtens, L. M. Augustin, T. de Vries, E. Smalbrugge, Y. S. Oei, R. Nötzel, R. Gaudino, D. J. Robbins, and M. K. Smit, "Monolithic AWG-based discretely tunable laser with nanosecond switching speed," presented at the 21st Annu. Meet. IEEE LEOS PD Session, Newport Beach, CA, 2008.

[8] *Spectral Grids for WDM Applications: DWDM Frequency Grid*, ITU-T G.694.1, May 2002.

[9] M. K. Smit and C. van Dam, "PHASAR-based WDM-devices: Principles, design and applications," *IEEE J. Sel. Topics Quantum Electron.*, vol. 2, no. 2, pp. 236–250, Jun. 1996.

[10] Y. A. Akulova, G. A. Fish, P.-C. Koh, C. L. Schow, P. Kozodoy, A. P. Dahl, S. Nakagawa, M. C. Larson, M. P. Mack, T. A. Strand, C. W. Coldren, E. Hegblom, S. K. Penniman, T. Wipiejewski, and L. A. Coldren, "Widely tunable electroabsorption-modulated sampled-grating (DBR) laser transmitters," *IEEE J. Sel. Topics Quantum Electron.*, vol. 8, no. 6, pp. 1349–1357, Nov./Dec. 2002.

[11] A. J. Ward, D. J. Robbins, G. Busico, E. Barton, L. Ponnampalam, J. P. Duck, N. D. Whitbread, P. J. Williams, D. C. J. Reid, A. C. Carter, and M. J. Wale, "Widely tunable DS-DBR laser with monolithically integrated SOA: Design and performance," *IEEE J. Sel. Topics Quantum Electron.*, vol. 11, no. 1, pp. 149–156, Jan./Feb. 2005.

[12] J.-O. Wesström, G. Sarlet, S. Hammerfeldt, L. Lundqvist, P. Szabo, and P.-J. Rigole, "State-of-the-art performance of widely tunable modulated grating Y-branch lasers," presented at the Opt. Fiber Commun. (OFC), Los Angeles, CA, Feb. 2004, Paper TuE2.

[13] J. H. den Besten, R. G. Broeke, M. van Geemert, J. J. M. Binsma, R. Heinrichsdorff, T. van Dongen, E. A. J. M. Bente, X. J. M. Leijtens, and M. K. Smit, "An integrated coupled-cavity 16-wavelength digitally tunable laser," *IEEE Photon. Technol. Lett.*, vol. 14, no. 12, pp. 1653–1655, Dec. 2002.

[14] J. J. M. Binsma, M. van Geemert, F. Heinrichsdorff, T. van Dongen, R. G. Broeke, E. A. J. M. Bente, and M. K. Smit, "MOVPE waveguide

regrowth in InGaAsP/InP with extremely low butt-joint loss," presented at the IEEE/LEOS Symp. Benelux Chapter, Brussels, Belgium, 2001.
[15] R. G. Broeke, J. J. M. Binsma, M. van Geemert, T. de Vries, Y. S. Oei, X. J. M. Leijtens, and M. K. Smit, "Monolithical integration of semiconductor optical amplifiers and passive modefilters for low facet reflectivity," presented at the IEEE/LEOS Symp. Benelux Chapter, Brussels, Belgium, 2001.
[16] Y. Barbarin, X. J. M. Leijtens, E. A. J. M. Bente, C. M. Louzao, J. R. Kooiman, and M. K. Smit, "Extremely small AWG demultiplexer fabricated on InP by using a double-etch process," *IEEE Photon. Technol. Lett.*, vol. 16, no. 11, pp. 2478–2480, Nov. 2004.
[17] B. Docter, F. Karouta, E. A. J. M. Bente, T. de Smet, and M. K. Smit, "Short-cavity lasers with deeply etched DBR mirrors for photonic integrated circuits," presented at the Symp. IEEE/LEOS Benelux Chapter, Twente, The Netherlands, 2008.
[18] R. Lang and K. Kobayashi, "External optical feedback effects on semiconductor injection laser properties," *IEEE J. Quantum Electron.*, vol. QE-16, no. 3, pp. 347–355, Mar. 1980.
[19] M. Yousefi and D. Lenstra, "Dynamical behavior of a semiconductor laser with filtered external optical feedback," *IEEE J. Quantum Electron.*, vol. 35, no. 6, pp. 970–976, Jun. 1999.
[20] B. Docter, E. J. Geluk, F. Karouta, M. J. H. Sander-Jochem, and M. K. Smit, "Deep etched DBR gratings in InP for photonic integrated circuits," in *Proc. 19th Int. Conf. Indium Phosphide Rel. Mater. (IPRM 2007)*, Matsue, Japan, pp. 226–228.
[21] B. Moeyersoon, J. Wittebolle, and G. Morthier, "Wavelength switching of semiconductor tunable lasers—How to suppress thermally induced wavelength drift," presented at the Symp. IEEE/LEOS Benelux Chapter, Amsterdam, The Netherlands, 2002.
[22] S. L. Woodward, P. Parayanthal, and U. Koren, "The effects of aging on the Bragg section of a DBR laser," *IEEE Photon. Technol. Lett.*, vol. 5, no. 7, pp. 750–752, Jul. 1993.

**Boudewijn Docter** (S'05–M'09) received the M.S. degree in electrical engineering from Twente University, Twente, The Netherlands, in 2002, and the Ph.D. degree from the Eindhoven University of Technology, Eindhoven, The Netherlands, in October 2009.

From 1998 to 2002, he was with BBV Software/Kymata/Alcatel Optronics, where he was engaged on design and simulation software for planar waveguide circuits. In 2003, he was with C2 V making arrayed waveguide grating (AWG) and variable optical attenuator (VOA) designs. He is currently with the Eindhoven University of Technology. His current research interests include application of photonic integrated circuits and tunable lasers in optical telecommunication networks.

Dr. Docter is a member of the IEEE Photonics Society.

**Jose Pozo** (M'10) was born in Barakaldo, Spain, in 1978. He received the B.Eng. and M.Sc. degrees in 2002 from the Universidad Publica de Navarra, Pamplona, Spain, and Vrije Universiteit Brussel, Brussels, Belgium, and the Ph.D. degree from the University of Bristol, Bristol, U.K.

In August 2007, he joined the COBRA Research Institute, Eindhoven, The Netherlands, where he was engaged in his research in the framework of the projects STW-TWICE and STW-EFFECT.

**Stefano Beri** was born in Imperia, Italy. He graduated in physics from Pisa University, Pisa, Italy, and Scuola Normale Superiore di Pisa, Pisa, in 2001 and received the Ph.D. degree in physics from Lancaster University, Lancaster, U.K.

He is currently a Postdoctoral Fellow of FWO-Vlaanderen with the Department of Applied Physics and Photonics and the Department of Physics, Vrije Universiteit Brussel, Brussels, Belgium.

**Ilya V. Ermakov** (S'05) was born in Novokuznetsk, Russia, in 1982. He received the degree in optoelectronic engineering (extraordinary award) from the Bauman Moscow State Technical University, Moscow, Russia, in 2005. In 2007, he became a Ph.D. student with the Universitat de les Illes Balears, Palma de Mallorca, Spain, and the Vrije Universiteit Brussel, Brussels, Belgium, where he is currently working toward the joint Ph.D. degree in laser physics.

His current research interests include complex dynamics of semiconductor lasers with optical feedback, chaos synchronization, and filtered optical feedback.

**Jan Danckaert** (M'04) was born in Antwerp, Belgium, in 1964. He received the Master's degree in physics from the University of Antwerp, Antwerp, in 1985, and the Ph.D. degree from the Vrije Universiteit Brussel (VUB), Brussels, Belgium, in 1992.

He then joined the Department of Applied Physics and Photonics (TONA), VUB, as a Teaching Assistant, where he was a Postdoctoral Research Fellow of the Research Foundation—Flanders (FWO). He was with INPG, Grenoble, France, during 1993. In 2001 and 2002, he was a Visiting Scientist with IMEDEA (now IFISC), UIB, Palma de Mallorca, Spain. Since 2005, he has been a Full-Time Professor with the VUB, where he is engaged in teaching introductory physics for both science and engineering students, and courses in photonics at the Master's level. His current research interests include semiconductor laser dynamics in general, vertical-cavity surface-emitting lasers, and semiconductor ring lasers in particular.

**Meint K. Smit** (A'93–M'00–SM'01–F'03) graduated in electrical engineering from the Delft University of Technology, Delft, The Netherlands, in 1974, and the Ph.D. degree in 1991, both with honors.

During 1974, he was engaged in radar and radar remote sensing. In 1976, he joined the Delft University of Technology, where he was engaged in research on integrated optics with special focus on optical communications in 1981. In 1994, he became a Leader of the Photonic Integrated Circuits Group, Delft University, and was appointed Professor in 1998. In 2002, he moved with his group to the Technical University of Eindhoven, Eindhoven, The Netherlands, where he is currently a Leader of the Opto-Electronic Devices Group, COBRA Research Institute.

Dr. Smit received a LEOS Technical Achievement award in 1997 for inventing the arrayed waveguide grating. In 2002, he was appointed LEOS Fellow for contributions in the field of opto-electronic integration.

**Fouad Karouta** (M'96–SM'98) received the Ph.D. degree from Montpellier University, Montpellier, France, in 1986.

In 1986, he joined the Eindhoven University of Technology, Eindhoven, The Netherlands, where he was engaged in various semiconductor materials like GaAs, InP, and GaN for optoelectronic and microelectronic applications. He has initiated or contributed to works on GaAs lasers, vertical-cavity surface-emitting lasers, high electron mobility transistors (HEMTs) and photoreceivers, and InP integrated optics including photonic crystals and GaN-based high-power HEMTs. Since March 2009, he has been with the Australian National University, Canberra, A.C.T., Australia, as Facility Manager of the Australian National Fabrication Facility A.C.T. Node, where he is engaged in GaAs, InP, GaN, and ZnO semiconductor materials.